AGU PUBLICATIONS

Geochemistry, Geophysics, Geosystems

RESEARCH ARTICLE

10.1002/2014GC005265

Effects of the core-shell structure on the magnetic properties of partially oxidized magnetite grains: Experimental and micromagnetic investigations

Kunpeng Ge[1,2], **Wyn Williams**[3], **Qingsong Liu**[1], **and Yongjae Yu**[4]

[1]State Key Laboratory of Lithospheric Evolution, Institute of Geology and Geophysics, Chinese Academy of Sciences, Beijing, China, [2]University of the Chinese Academy of Sciences, Beijing, China, [3]School of GeoSciences, University of Edinburgh, Edinburgh, UK, [4]Department of Geology and Earth Environmental Sciences, Chungnam National University, Daejeon, South Korea

Abstract The relationship between magnetic hysteresis parameters and the degree of oxidation of ultrafine magnetite particles is examined by both experimental measurements (distributed particle assemblage with median grain size of ∼80 nm and standard deviation 0.43) and micromagnetic simulations (single particles from 40 nm to 140 nm). Experimental results show that both coercivity (B_c) and the ratio of saturation remanence to saturation magnetization (M_{rs}/M_s) increase slowly, as the oxidation parameter z increases from 0 to ∼0.9. Thereafter, both parameters decrease sharply as magnetite becomes completely oxidized to maghemite. Numerical simulations of hysteresis loop and microstructure using a micromagnetic model with a core-shell geometry (a stoichiometric core surrounded by an oxidized shell) show three categories of behavior for magnetic grains during oxidation. First, the coercivity of SD particles decreases as oxidation proceeds, but their remanence magnetization remains in a uniform state. Second, for PSD sized particles near the critical SD boundary (80 nm to 100 nm), the initial vortex domain structure changes to a SD as oxidation occurs and returns to a vortex state upon complete maghemitization, resulting in an initial rise and then fall of B_c and M_{rs}. Finally, larger PSD grains remain a vortex state throughout the maghemitization, with less variations of B_c and M_{rs}. The predicted magnetic properties exhibit good agreement with experimental observations and suggest that the domain arrangement is likely to be dominated by a core-shell structure with strong exchange coupling at their interface. Overall, the partially oxidized magnetite in SD-PSD range can reliably record palaeomagnetic signals.

Special Section:
Magnetism From Atomic to Planetary Scales: Physical Principles and Interdisciplinary Applications in Geo- and Planetary Sciences

Key Points:
- The low-temperature oxidation is very common in natural environments
- Experiments and micromagnetic modeling are studied
- The partially oxidized magnetite can record palaeomagnetic signals

Correspondence to:
Q. Liu,
qsliu@mail.iggcas.ac.cn

Citation:
Ge, K., W. Williams, Q. Liu, and Y. Yu (2014), Effects of the core-shell structure on the magnetic properties of partially oxidized magnetite grains: Experimental and micromagnetic investigations, *Geochem. Geophys. Geosyst.*, *15*, 2021–2038, doi:10.1002/2014GC005265.

Received 28 JAN 2014
Accepted 22 APR 2014
Accepted article online 27 APR 2014
Published online 30 MAY 2014

1. Introduction

The chemical changes in magnetic iron oxides that occur below their magnetic ordering temperature, have long been of interest to palaeomagnetic workers [*Johnson and Merrill*, 1972, 1974; *Moskowitz*, 1980; *Özdemir et al.*, 1993; *Özdemir and Dunlop*, 2010]. It has been known that low temperature oxidation of magnetite or titanomagnetite is ubiquitous in nature, which can take place in basalts [*Prévot et al.*, 1981; *van Velzen and Dekkers*, 1999], loess [*Liu et al.*, 2004, 2007], red sandstones [*Liu et al.*, 2011], and soils [*C C Liu et al.*, 2010; *Liu et al.*, 2012; *Lu et al.*, 2012]. Low temperature oxidation of titanomagnetite particles in the oceanic crust is likely to complicate its natural remanent magnetization (NRM), such as in marine magnetic anomalies where much of the seafloor carries no thermal remanent magnetization (TRM) at all [*Marshall and Cox*, 1971; *Özdemir and Dunlop*, 1985; *Smith*, 1987; *Xu et al.*, 1997; *Wang et al.*, 2006]. Long periods of oxidation after cooling of rocks may cause large changes in their remanence direction and intensity, and hence significantly affect the understanding of Earth geomagnetic field [*Watkins*, 1967; *Gallagher*, 1968; *Johnson and Merrill*, 1973; *Haneda and Morrish*, 1977; *Özdemir and Dunlop*, 1985, 2010; *Cui et al.*, 1994].

Low-temperature oxidation of titanomagnetite occurs as a weathering process under natural atmospheric conditions [*Özdemir and Dunlop*, 1985; *van Velzen and Dekkers*, 1999; *Liu et al.*, 2010]. The oxidation process starts at its surface, where Fe^{2+} is oxidized to Fe^{3+}. Fe^{2+} is either partially removed from the crystal or it reacts with oxygen to form a new crystal layer [*O'Reilly*, 1984]. Further oxidation is a diffusion process driven by the oxidation gradient where Fe^{2+} diffuses from the interior of the grain to the surface, leaving vacancies in the interior. Because of the isolation effect of the oxidized layer and the rapid reduction of the solid state diffusion coefficient at low temperature [*Gallagher*, 1968; *Askill*, 1970], a strong oxidation gradient builds up close to the grain surface. As a result, an oxidized shell is formed around an unoxidized core (so called the core-shell structure).

The core-shell structure has been studied since the 1960s [*Gallagher*, 1968; *Banerjee et al*., 1981; *Özdemir and Dunlop*, 1993, 2010; *Cui et al*., 1994; *van Velzen and Dekkers*, 1999; *Liu et al*., 2004], using different methods (e.g., X-ray diffraction, chemical analysis, Mössbauer spectroscopy, magnetic measurements). In particular, *Cui et al*. [1994] provided three possible explanations for the pseudo-single-domain (PSD) behavior of the multidomain (MD) grains with an oxidized surface. First, that magnetization is dominated by the PSD-like core of the grain, which is independent of the shell. Second, the stress due to the mismatches of the cell dimensions on either side of the phase boundary (not modeled in the present study) will increase the domain wall energy and make it difficult to add domain walls, thus favoring the nucleation of PSD-like structures. The third suggestion is that the mixture effect of single-domain (SD) maghemite and the MD magnetite might yield an overall PSD-like behavior.

Liu et al. [2004] investigated the surface oxidized particles of PSD/MD size obtained from Chinese loess, and found that the minerals exhibited a well-defined Verwey transition [*Özdemir et al*., 1993; *Cui et al*., 1994] suggesting that the highly diminished magnetite core still remains stoichiometric even after being heated to 700°C. Such observation indicates that the magnetite core remains fairly stable during varying chemical and physical conditions. *Özdemir and Dunlop* [2010] suggested a low-temperature method to investigate the oxidation state of magnetite and considered that a transition zone may exist between the maghemite shell and the magnetite core, where the lattice parameters gradually change. Regardless of these attempts, relatively few experimental studies have been conducted on maghemitization, with the notable exception of *Özdemir and Dunlop* [2010], and details of how the core-shell structure affects the magnetic behavior of the partially oxidized magnetic particles remain poorly understood.

The micromagnetic modeling is an effective method to examine the processes of magnetization in small particles [*Schabes and Bertram*, 1988; *Williams and Dunlop*, 1989; *Fidler and Schrefl*, 2000]. In recent years, numerous micromagnetic studies have been carried out to establish the magnetic properties and domain states of magnetite nanocrystals focusing on grain morphology [e.g., *Williams and Dunlop*, 1989; *Witt et al*., 2005; *Williams et al*., 2006, 2010, 2011; *Yu and Tauxe*, 2008], the effects of interactions between particles [*Muxworthy et al*., 2003, 2004; *Yu and Tauxe*, 2005], and the critical grain sizes for different domain states [*Williams and Dunlop*, 1989, 1995; *Fabian et al*. 1996; *Muxworthy et al*., 2004]. However, few micromagnetic studies have attempted to investigate the inner structure of multiphase iron oxides; and although the core-shell model has already been introduced for MD and large PSD grains [*Cui et al*., 1994; *Özdemir and Dunlop*, 2010], little is known regarding the magnetization structure or how it couples with the oxidized surface for the palaeomagnetically important SD and small PSD grain sizes.

This study aims to investigate the effects of oxidation on the magnetic properties of finer grained magnetite by integrating micromagnetic simulation and experimental results. The significances and caveats of the micromagnetic modeling results will be further discussed.

2. Samples and Experiments

Experimental samples were obtained from a commercial magnetite powder (number code 4000 manufactured by the Wright company), which contains a relatively narrow range of SD and PSD grain sizes. Transmission electron microscopy (TEM) observations were carried out on a JEM-2100 microscope with an accelerating voltage of 200 kV. The particles are clumped (Figure 1a) but still can be clearly counted from the margin of the clusters. The grain size distribution was determined from a total of 1177 particles counted from more than 20 TEM images. To estimate the particle dimensions, distribution of major axis m, minor axis n, and natural logarithm of equivalent circular diameter d (where $d=2(m \cdot n/\pi)^{1/2}$) are shown (Figures 1b–1d). The grain size distribution is heavily biased toward smaller grain sizes, resembling a lognormal distribution.

In order to reduce any pre-existing surface oxidation and obtain the stoichiometric magnetite crystals, the initial samples were heated in a mixture of 80% CO_2 and 20% CO at 395°C for 74 h [*Özdemir and Dunlop*, 2010]. Samples were then oxidized in air by heating to different temperatures for various periods of time. Five different temperatures were used (50, 100, 150, 200, and 250°C), and with five different heating periods

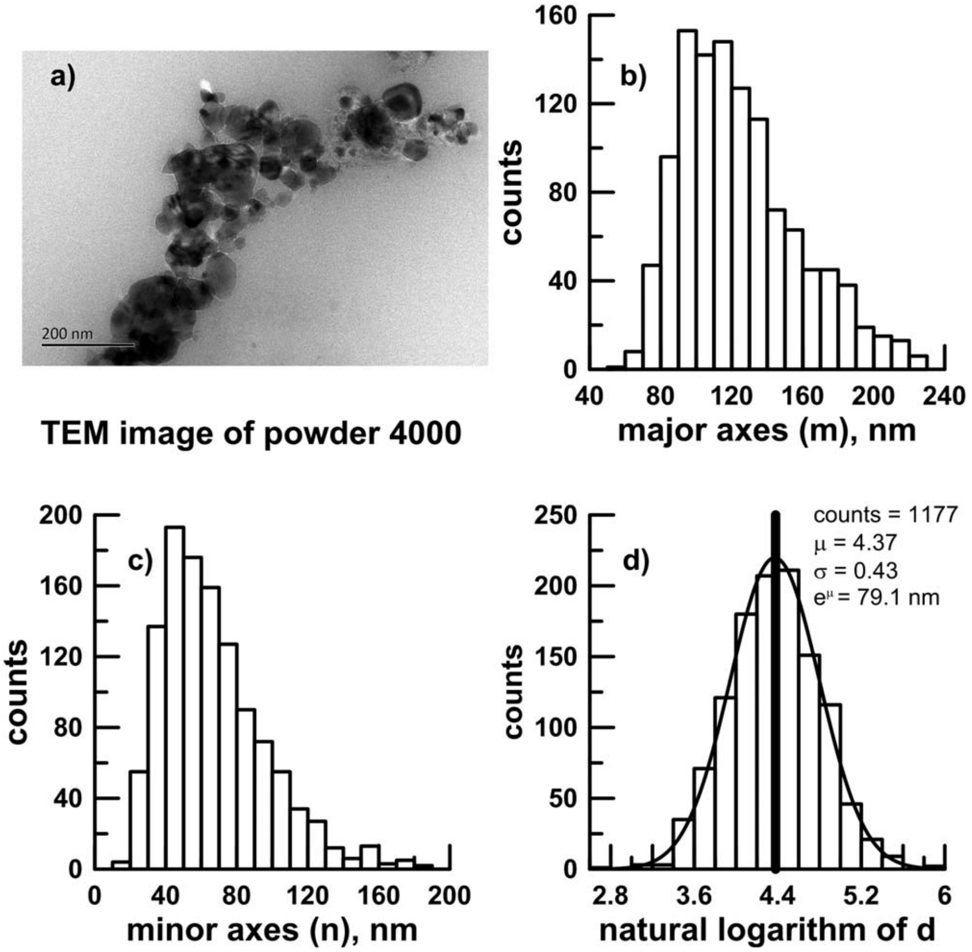

Figure 1. (a) TEM image of the magnetic powder 4000. (b–d) Distributions of major axes m, minor axes n, and natural logarithm of the mean grain size *d* determined from counts in TEM photos for powder 4000. The heavy black line in Figure 1d indicates the median value. The curve in Figure 1d shows a normal distribution fitting of the histograms. Statistically, the mean value and standard deviation of the logarithm of mean grain size are 4.37 and 0.43, respectively, representing a middle grain size of 79.1 nm.

at each temperature (1, 1.5, 2, 2.5, and 3 h) which, together with the initial magnetite, produces a total of 26 different samples. The detailed processing sequence can be referred in Table 1.

The oxidation parameter z was defined from the following formula [*Readman and O'Reilly*, 1971]

$$\mathrm{Fe}^{2+} + (z/4)\mathrm{O}_2 \rightarrow (1\text{-}z)\mathrm{Fe}^{2+} + z\mathrm{Fe}^{3+} + (z/2)\mathrm{O}^{2-}$$

where the oxidation parameter z varies from 0 to 1, representing a transformation from magnetite ($z = 0$) to maghemite ($z = 1$).

X-ray diffraction (XRD) is one of the logical methods to estimate the cell edge parameter, which is strongly dependent upon the oxidation parameter [*Özdemir et al.*, 1993; *Özdemir and Dunlop*, 2010]. The superstructure reflections for maghemite could be easily identified by XRD, but do not exist in magnetite (and titanomagnetite).

Cell edges for all these powder samples were first measured from XRD analysis on a Philips X'Pert diffractometer with the Cu-Kα radiation operated at 40 kV and 40 mA. By comparing the standard power diffraction file (PDF) of magnetite (PDF#19-0629) and maghemite (PDF#39-1346), the cell sizes and errors were then determined by the "cell refinement method" [*Rietveld*, 1969] using the jade software version 6.5. Finally, the oxidation parameters were calculated by least squares fitting with the corrected curves [*Readman and O'Reilly*, 1972] of cell size versus oxidation parameter z.

Table 1. Hysteresis Parameters (B_c and M_{rs}/M_s) for Stoichiometric and Partially Oxidized Magnetite and Maghemite[a]

Sample	Temperature (°C)	Time (h)	a (Å)	Error (Å)	z^b	B_c (mT)	M_{rs}/M_s	M_s (A m^2/kg)
y0			8.390	0.002	0.00	18.3	0.233	82.4
y501	50	1	8.370	0.002	0.59	17.4	0.225	72.4
y5015	50	1.5	8.379	0.003	0.39	18.0	0.230	74.5
y502	50	2	8.401	0.001	0.00	18.1	0.233	81.0
y5025	50	2.5	8.386	0.003	0.16	16.7	0.222	79.1
y503	50	3	8.389	0.002	0.08	17.6	0.224	80.8
y1001	100	1	8.374	0.003	0.50	18.3	0.234	72.2
y10015	100	1.5	8.382	0.001	0.29	18.5	0.235	75.5
y1002	100	2	8.357	0.004	0.84	18.7	0.240	65.4
y10025	100	2.5	8.386	0.004	0.17	18.9	0.237	78.9
y1003	100	3	8.386	0.002	0.18	18.7	0.237	78.7
y1501	150	1	8.381	0.003	0.31	19.4	0.253	76.0
y15015	150	1.5	8.362	0.004	0.76	19.9	0.249	67.0
y1502	150	2	8.372	0.007	0.56	20.3	0.257	70.9
y15025	150	2.5	8.379	0.001	0.38	19.2	0.253	74.7
y1503	150	3	8.346	0.002	0.95	21.2	0.264	63.1
y2001	200	1	8.350	0.002	0.91	20.1	0.278	63.8
y20015	200	1.5	8.328	0.003	0.99	19.6	0.274	69.0
y2002	200	2	8.342	0.002	0.96	15.9	0.254	62.8
y20025	200	2.5	8.348	0.001	0.93	17.7	0.264	63.5
y2003	200	3	8.333	0.003	0.97	17.3	0.255	66.6
y2501	250	1	8.330	0.003	0.99	14.2	0.227	62.8
y25015	250	1.5	8.342	0.002	0.96	14.4	0.223	62.7
y2502	250	2	8.342	0.003	0.96	14.1	0.227	64.8
y25025	250	2.5	8.341	0.009	0.97	14.1	0.226	62.7
y2503	250	3	8.323	0.003	0.99	14.3	0.230	63.6

[a] Chemical processing environments (temperature and time period), the corresponding spinel cell edge parameters and their saturation magnetization are also listed.

[b] Oxidation parameter z, as defined in the text, was obtained by comparing the measured values of X-ray cell edge *a* with the calibration curve *Readman and O'Reilly* [1972].

These samples were subsequently dispersed into KBr matrices (mean grain size 10 μm) at about 0.5% by weight. Hysteresis loops were then measured on MicroMag 3900 Vibrating Sample Magnetometer (VSM; Princeton Measurements Corp., USA) at room temperature with field ranging from -1.0 to 1.0 Tesla.

3. Micromagnetic Modeling

In this study, we use a core-shell model to investigate the process of low-temperature oxidation. The model subdivides a grain into a number of discrete subcubes (Figure 2a) with edges along [100] crystallographic direction. In order to investigate the effects of the separated layers, a shell-only model (Figure 2b) and its corresponding core-only model were also investigated.

The finite-difference (FD) micromagnetic model is used to calculate stable magnetic structures by a dual approach [*Muxworthy et al*., 2004; *Muxworthy and Williams*, 2006; *Williams et al*., 2006]. First, the free magnetic energy E_{total} is minimized. This energy is the sum of the exchange energy E_{ex}, the magnetostatic energy E_d, the magnetic crystalline anisotropy E_{anis} [*Brown*, 1963] and the external field energy E_{h} as follows

$$E_{total} = E_{ex} + E_{anis} + E_d + E_h$$

From the minimum energy solution, the final equilibrium domain state can be obtained by minimizing the torque that the effective field ($\boldsymbol{H}_{eff}$) exerts on the magnetization, determined by integrating the Landau-Lifshitz-Gilbert (LLG) equation

$$\frac{d\boldsymbol{M}}{dt} = -\frac{\gamma}{1+\alpha^2}\boldsymbol{M}\times\boldsymbol{H}_{eff} + \frac{\alpha\gamma}{(1+\alpha^2)M_S}\boldsymbol{M}\times(\boldsymbol{M}\times\boldsymbol{H}_{eff})$$

where $\boldsymbol{M}$ is the unit vector along the magnetization direction, γ is the gyromagnetic ratio, and α is a damping parameter. $\boldsymbol{H}_{eff}$ is the effective field acting on the vector at each node of the finite element mesh defined as

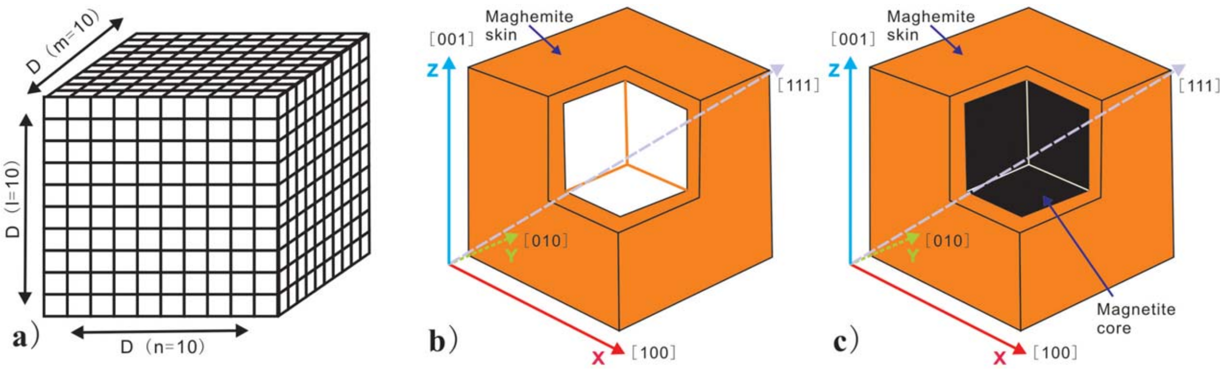

Figure 2. Frame of reference for micromagnetic modeling. (a) Discretization scheme of the particle showing the number of cells along the width n, length l, and thickness m. (b) The shell-only model with crystallographic axes [001], [010], [100], [111], with radial section to the center. The shell-only model was built using a cubic skin (colored brown above) with hollow interior, representing a maghemite shell-only structure. (c) The core-shell model with crystallographic axes [001], [010], [100], [111], with radial section to the center. The core-shell model was built using a cubic skin (brown) and a cubic interior (black), representing the maghemite shell and the magnetite inner core, respectively.

$$\boldsymbol{H}_{eff} = \frac{dE_{total}}{d\boldsymbol{M}}$$

In the core-shell model, the magnetite and maghemite regions were defined by setting the relevant material parameters (Table 2) for each element in the geometry (Figure 2c). Both magnetite and maghemite share the same easy magnetization axis [111]. The strength of the exchange coupling across the phase boundary between magnetite and maghemite was varied independently.

In this study, we use a very simple micromagnetic model to examine the extent to which the experimental observations can be explained in terms of magnetostatic and exchange coupling across the boundary in a core-shell multiphase model. The numerical model neglects dislocations or other defects, and in particular ignores the effects of stress caused by the crystal cell size mismatch at the phase boundary.

The model also does not include the effects of thermal fluctuations. Therefore, models with a superparamagnetic (SP) grain size magnetite core in the uncoupled core-shell and core-only models, which occur for large shell thickness, representing a much higher oxidation state, were not calculated. Although thermal fluctuations are unlikely to change the available equilibrium magnetization structures, the estimated coercivity will be reduced by values ∼10 mT for magnetite [*Dunlop and Özdemir*, 2001]. Magnetostriction was also not considered since its effects are not significant for magnetite particles smaller than 0.5 μm in size [*Fabian et al.*, 1996].

For the core-shell model, the exchange constant (C_E) at the boundary [*Johnson and Merrill*, 1974] is unknown, and thus three possibilities are considered (i) a value of 0 J m^{-1} across the boundary which represents an exchange uncoupled model, (ii) a relatively small value of 5×10^{-12} J m^{-1}, which represents a weak interaction due to the potential mismatch across the boundary, and (iii) a sensible average of the two exchange constants for the different materials, namely 1.17×10^{-11} J m^{-1}.

Simulations of hysteresis loops were performed by computing the quasi-static domain structures and resulting field-aligned magnetization for field values between +80 mT and −80 mT in 5 mT steps. Values for the coercive force (B_c) and the ratio of saturation remanence to saturation magnetization (M_{rs}/M_s) are obtained by averaging the modeling results from fields aligned along the easy [111], hard [100] and intermediate [110] directions.

We considered grains of six volumes: 0.64×10^{-22}, 2.16×10^{-22}, 5.12×10^{-22}, 10×10^{-22}, 17.28×10^{-22}, and 27.44×10^{-22} m^3, corresponding to cubes with edge lengths of 40, 60, 80, 100, 120, and 140 respectively, which cover the range from stable SD to PSD state for both magnetite and maghemite.

Table 2. Principle Magnetic Constants, Namely Saturation Magnetization, M_s, Magnetocrystalline Anisotropy, K_1, and Exchange Constant C_E for Magnetite and Maghemite used in the micromagnetic modeling

Mineral	M_s (A m^{-1})	K_1 (J m^{-1})	C_E (J m^{-1})
Magnetite[a]	4.8×10^5	-1.24×10^4	1.34×10^{-11}
Maghemite[b]	3.8×10^5	-4.6×10^3	1×10^{-11}

[a] Material parameters from *Pauthenet and Bochirol* [1951] and *Heider and Williams* [1988].

[b] Material parameters from *Hou et al.* [1998] and *Dunlop and Özdemir* [2001].

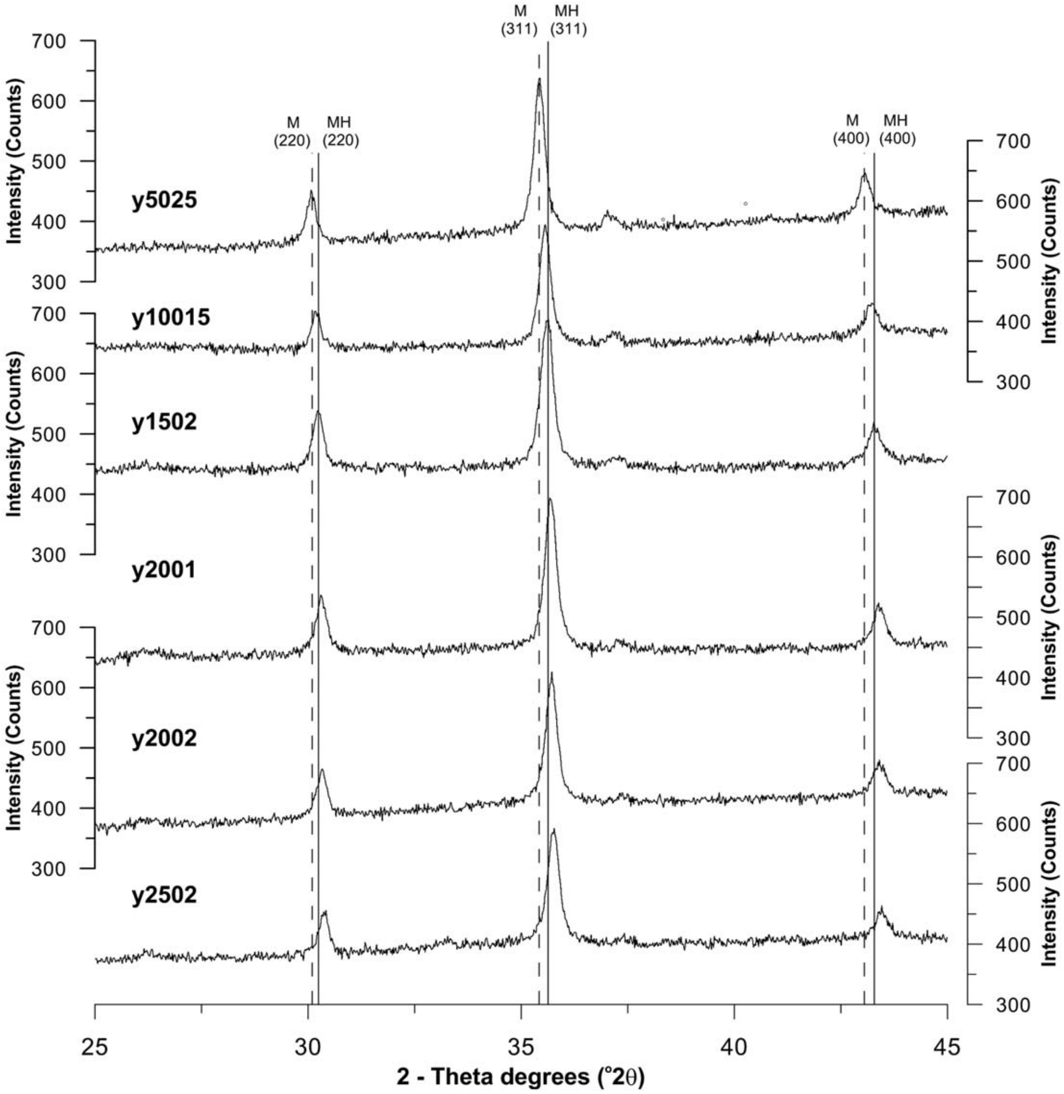

Figure 3. XRD spectrum for magnetic extracts of typical oxidized samples, with z equal to 0.16, 0.29, 0.56, 0.91, 0.96, and 0.97, see detailed information in Table 1. The labels M, MH are for magnetite and maghemite respectively. The dashed lines drawn around 30.10° (*hkl*, 220), 35.42° (*hkl*, 311), and 43.05° (*hkl*, 400) represent the dominant peaks of magnetite. And three characteristic solid lines at 30.24° (*hkl*, 220), 35.63° (*hkl*, 311) and 43.28° (*hkl*, 400) are the peaks of maghemite.

The different degrees of oxidation were modeled by varying the shell thickness, and the oxidation parameter z obtained by a volume fraction of the oxidized shell to total grain volume. In this way, we considered four different oxidized states, namely z- values of 0.271, 0.488, 0.784, and 0.992. Including the two end members (100% magnetite and maghemite), a total of 108 different core-shell models were generated. In addition to the core-shell models, the shell-only and the core-only models were also calculated in this study. The oxidation parameters of shell-only and core-only models are stated as if the shell or core were part of a complete core-shell structure. Including the four oxidized states, a total of 24 shell-only and 24 core-only models were calculated.

4. Results

4.1. Experimental Results

The stoichiometric magnetite samples were shiny black in appearance, the partially oxidized magnetite powders were black and gray, and the powders that had a high degree of oxidation were brown in color reflecting the presence of maghemite. The magnetic properties and X-ray cell edge parameters of

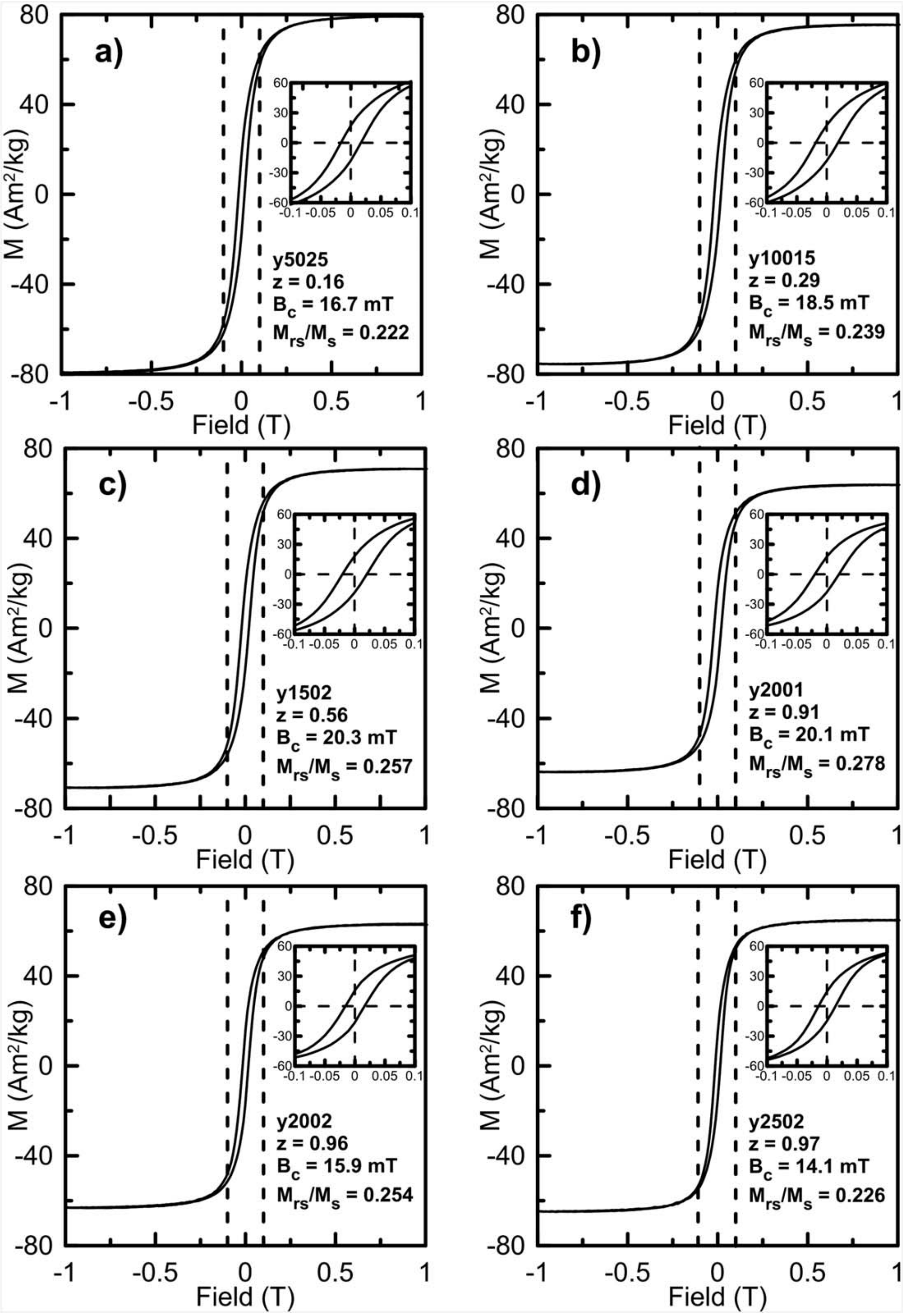

Figure 4. Representative hysteresis loops of typical oxidized samples demonstrated in Figure 3, namely with z equal to (a) 0.16, (b) 0.29, (c) 0.56, (d) 0.91, (e) 0.96, and (f) 0.97, measured at room temperature with paramagnetic correction. Details of the hysteresis behavior near the origin (between the two dashed black lines) are shown in the top right of each figure.

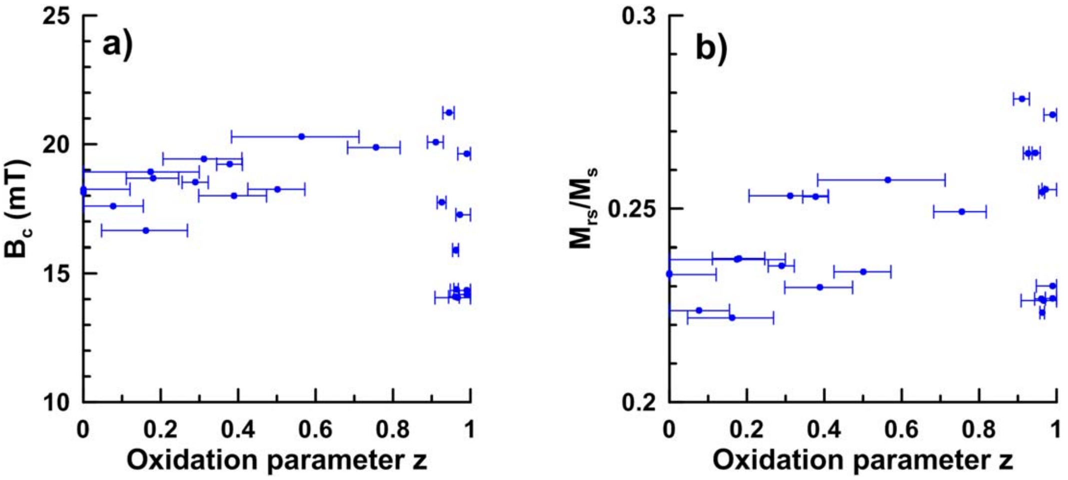

Figure 5. Experimental observation of (a) coercive field (B_c) and (b) ratio of saturation remanence to saturation magnetization (M_{rs}/M_s), versus oxidation parameter z for dispersed powders. The error bars of the data show the errors of oxidation parameter generated by XRD measurements.

stoichiometric (reduced) and oxidized magnetite are given in Table 1. The oxidation parameter is very sensitive to temperature and heating periods below 200°C. Powder heated with temperature higher than 200°C will be highly oxidized ($z > 0.9$). In general, the oxidation parameter increases with temperature, but no simple relationship for the heating period was observed. However, the statistical variance of the oxidation parameter z from 0 to 1 can still be obtained under a comprehensively varying chemical environment.

The mineralogical identification of magnetite powders was performed based on the data between 15° and 65° (2θ) in XRD measurements. Six typical XRD experimental spectra are shown (simplified with 2θ from 25° to 45°) in Figure 3, for $z = 0.16$, 0.29, 0.56, 0.91, 0.96, and 0.97. A gradual shift of peaks from magnetite to maghemite can be distinguished clearly as the oxidation parameter becomes larger. The corresponding hysteresis loops after paramagnetic slope corrections are shown in Figure 4. All the powders are magnetically saturated before 500 mT (Figure 4), which is close to the expected SD behavior for an assemblage of magnetic particles [*Tauxe et al*., 2002; *Fukuma and Dunlop*, 2006]. The reductions of saturation magnetization (M_s) indicate the gradual changes from magnetite to maghemite during oxidation. The squareness ratios (M_{rs}/M_s) of the hysteresis loops become wider when $z < 0.91$ (Figure 4d), as well as producing wider hysteresis loops. For $z > 0.91$, the coercivity and squareness ratio decrease rapidly as loops become thinner.

Changes in B_c and M_{rs}/M_s with respect to the oxidation parameter z are illustrated in Figure 5. The deviations of the oxidation states were generated by measurement uncertainties of lattice size in the XRD analysis (Table 1), which were directly related to the oxidation parameter z. Compared to high oxidation states, the lower oxidization parameters of magnetic powders have greater uncertainties, because z is more sensitive to the variations of cell edge at the beginning of maghemitization [*Readman and O'Reilly*, 1972]. Overall, B_c and M_{rs}/M_s share a similar trend, although M_{rs}/M_s versus z is more scattered than the coercivity. There is a steady increase of B_c and M_{rs}/M_s up to $z = \sim 0.9$, ranging from ~17 to ~21 mT for B_c, and ~0.22 to ~0.28 for M_{rs}/M_s, respectively. A sharp decrease in both parameters is observed when $z > 0.9$.

4.2. Shell-Only and Core-Only Models

For both SD (40 and 60 nm) and PSD (80, 100, 120, and 140 nm) size particles, their hysteresis parameters versus oxidation parameter of the shell-only model (Figures 6a and 6b) are strikingly different. The coercivity of both SD and PSD particles decrease gradually with respect to z when $z < 0.8$, and thereafter the coercivity decreases continually for SD grains, but generally increases for the PSD grains. The M_{rs}/M_s ratio for SD particles is almost independent of the oxidation degree. However, for PSD grains the ratio decreases with increasing oxidation when $z < 0.8$, which is similar to the behavior of B_c.

The hysteresis properties versus oxidation parameters for the core-only model of SD and PSD grains appear to be more complicated than the shell-only model (Figures 6c and 6d). The core-only models are essentially

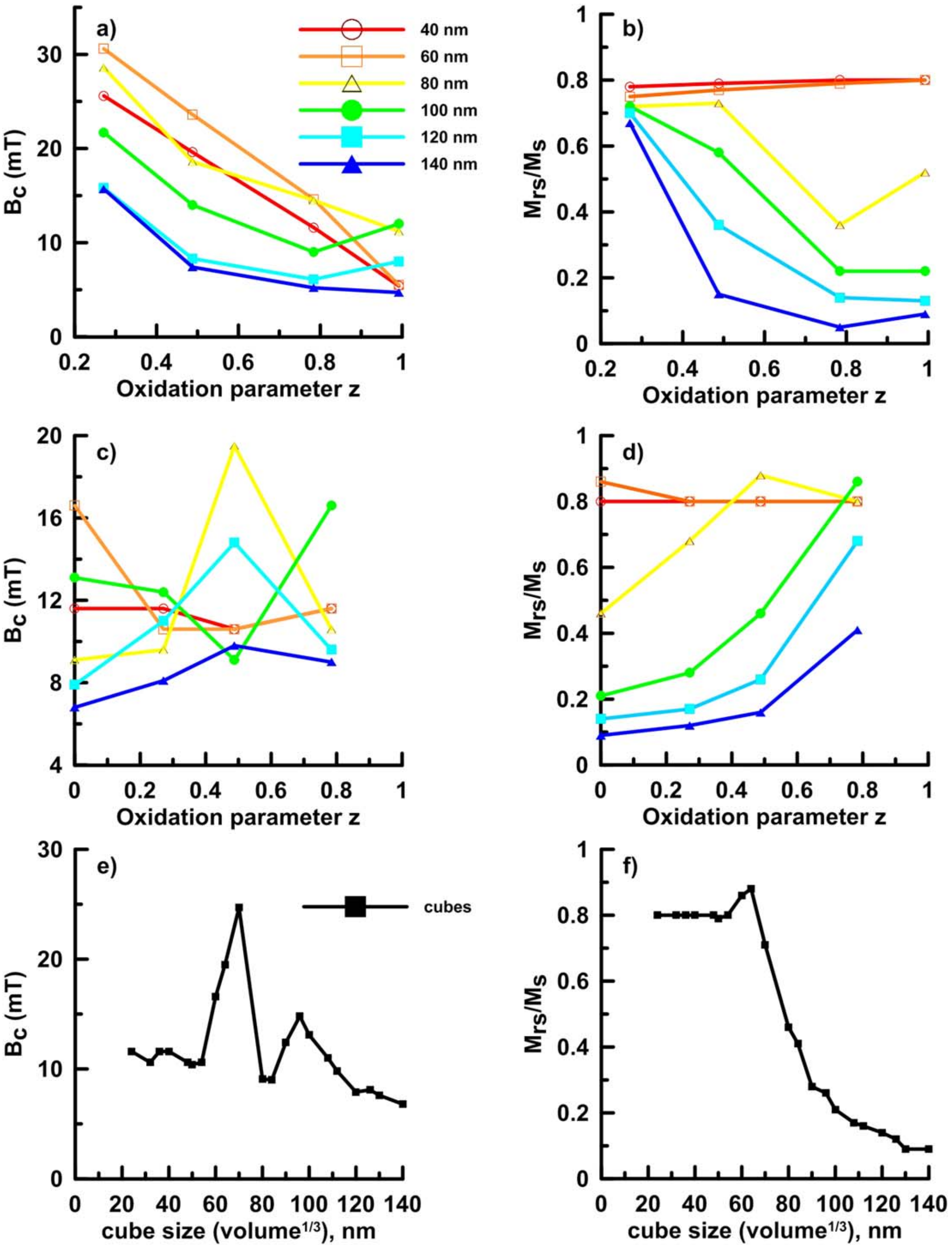

Figure 6. Micromagnetic predictions for B_c and M_{rs}/M_s versus oxidation parameter z (represent) for the (a and b) shell-only models and (c and d) core-only models. (e and f) B_c and M_{rs}/M_s of cubic magnetite as functions of grain size. The oxidation parameters were calculated as if the shell and core were part of a complete core-shell structure. Hysteresis parameters versus z for each grain size were colored according to the color bar in Figure 6a.

just different size cubic magnetites, the hysteresis parameters of which are functions of grain size, as illustratively shown in Figures 6e and 6f [*Williams et al.*, 2006]. As the oxidation degree increases, the grain size of the core decreases to small SD size or nearly SP size for SD grains (40 nm and 60 nm), and to stable SD size for PSD grains. A reduction in the coercivity of the core for SD grain is observed because of the decrease of magnetic energy. The decrease in coercivity with reduced grain size from SD particles ($<$ 70 nm), due to a decrease in the amount of “flowering” of magnetization near the surfaces, can be seen in Figure 6e. The variation of coercivity versus oxidation parameter of the core in PSD size grains exhibits typical characteristic of magnetite ranging from small PSD to stable SD cubic grain. The squareness ratios of core-only models remain constant for SD grains and increases steadily in PSD grains (Figures 6d–6f).

4.3. Core-Shell Model

The hysteresis results for the core-shell model with different exchange values are shown in Figure 7. Magnetic properties of the exchange uncoupled model show dramatic changes as the oxidation parameter increases, and is quite distinct from the trend observed for the shell-only and core-only models (Figures 7a and 7b). The negative hysteresis parameters obtained at $z = \sim 0.5$ (where we have near equal strength magnetization in the core and shell) for grains around the SD/PSD size (60, 80, and 100) are due to the magnetostatic interactions between the core and shell. This produces a back-field that promotes asynchronous switching of the uncoupled parts, (i.e., the magnetic core switches first followed by the shell) and it can result in the switching of the overall remanence of the particle before the external field has switched. This did not happen for smaller SD (40 nm) and larger PSD particles (120 and 140 nm) because either the back-field here was not large enough or the core was relatively stable, resulting in positive hysteresis parameters at $z = \sim 0.5$. By using the model parameters (i.e., hysteresis parameters for modeled particles with grain sizes of 40, 60, 80, 100, 120, and 140 nm) to represent the median average values with a bin of 20 nm based on the distribution shown in Figure 1, hysteresis properties of a distributed model with grain sizes ranging from 30 nm to 150 nm could be simulated to a first-order approximation. Again, the case with $z > 0.8$ was not modeled because the uncoupled core is less than the superparamagnetic grain size.

The hysteresis properties of coupled model versus oxidation parameter with exchange values of 5×10^{-12} and 1.17×10^{-11} J m^{-1} at the interface are shown in Figures 7c–7f. Compared with the uncoupled model, the coupled models display similar results and yield smoothly varying hysteresis properties. The predicted magnetic properties, i.e., the weighted parameters of the coupled models based on the distribution of experiment measurements (Figure 1), in particular the squareness ratios trend, agrees well with the experimental observations. It indicates that the exchange coupling between the core and the shell plays a dominant role in controlling the magnetic properties of the oxidized particles. The core-shell structure generally displays a gradual reduction of coercivity through the whole process of oxidation for SD particles (Figures 7c and 7e), while the corresponding M_{rs}/M_s values are unchanged (Figures 7d–7f).

For the PSD grains, the overall trend is for both B_c and M_{rs}/M_s to increase as a function of oxidation up to $z = \sim 0.9$ at which point a dramatic decrease in both hysteresis parameters is observed (Figures 7c and 7e). Within this overall trend, the small PSD grains near the PSD/SD grain size boundary (80 and 100 nm) show a greater variability than do the larger PSD (120 and 140 nm) grains.

4.4. Micromagnetic Structures

The stable M_{rs}/M_s throughout the wide range of z values for the core-shell models of SD grains (Figures 7d–7f) indicates that the micromagnetic structures remain uniform during the whole oxidation process. However, magnetic behaviors for remanence structures of shell-only models (Figure 8) are more complicated. The magnetization structure aligns parallel to the plane of the skin and is uniform for small grains or low values of oxidation. As the oxidation parameter increases, a vortex structure is nucleated within the oxidized skin (Figures 8c and 8d).

Micromagnetic structures of core-shell model, which considered the average exchange value at the interface (i.e., 1.17×10^{-11} J m^{-1}), are displayed in Figures 9 and 10. Figure 9 shows typical zero-field micromagnetic core-shell structures for 60 and 100 nm grains at $z = 0$ and at $z = 0.488$, respectively. Compared with the stoichiometric magnetite, the remanence state of the surface oxidized grain is more uniform (Figures 9a and 9b). For 100 nm size grain (Figures 9c and 9d), the only stable remanence state nucleated is that of a vortex. However, the magnetization is more symmetrical, with a more uniform outer shell compared to the model for the stoichiometric magnetite.

The zero-field magnetic structures (remanence state) as a function of oxidation parameter for the 80 nm grain are shown in Figure 10. The stoichiometric magnetite shows a vortex structure. As the oxidation parameter increases, the vortex structure becomes more uniform and the volume of the core also increases.

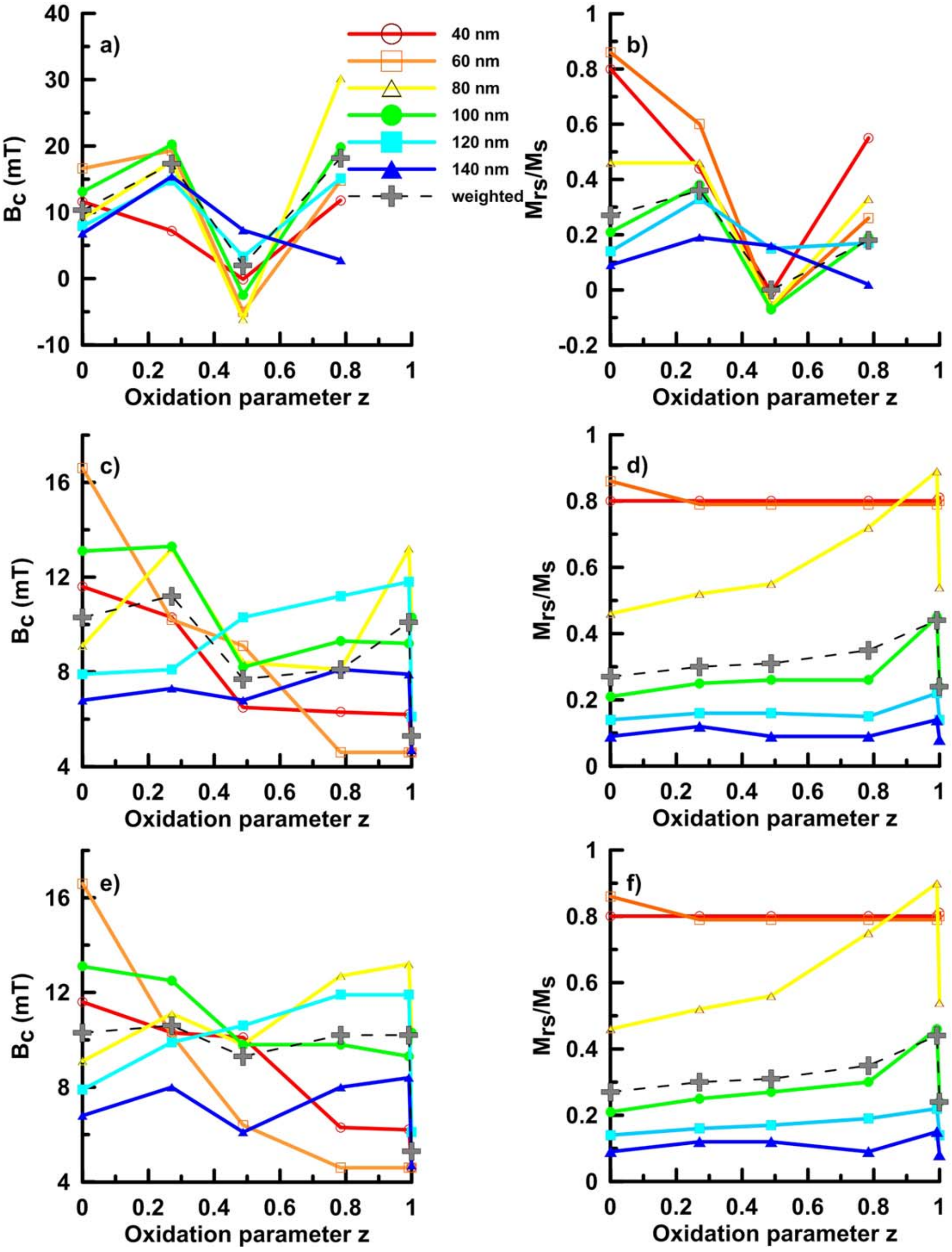

Figure 7. Micromagnetic results of coercive field (B_c) and ratio of saturation remanence to saturation magnetization (M_{rs}/M_s) versus oxidation parameter z for models with different exchange values at the core-shell boundary. Hysteresis parameters versus z for each grain size were colored according to the color bar in Figure 7a. The black dashed lines with gray crosses show weighted values of model curves based on the distribution shown in Figure 1. The hysteresis parameters of (a and b) exchange uncoupled and (c–f) exchange coupled models were modeled by the core-shell model with exchange values of 0, 5×10^{-12} and 1.17×10^{-11} at the boundary, respectively. Note that cases for exchange uncoupled models with high oxidation parameter ($z > 0.8$) were not calculated as the corresponding inner core would be within the superparamagnetic grain size range.

However, the magnetic structure becomes approximately uniform when $z = \sim 0.8$, and becomes increasingly uniform as the oxidation parameter grows. Finally, the magnetic structure returns to a vortex state when the particle is totally oxidized to maghemite.

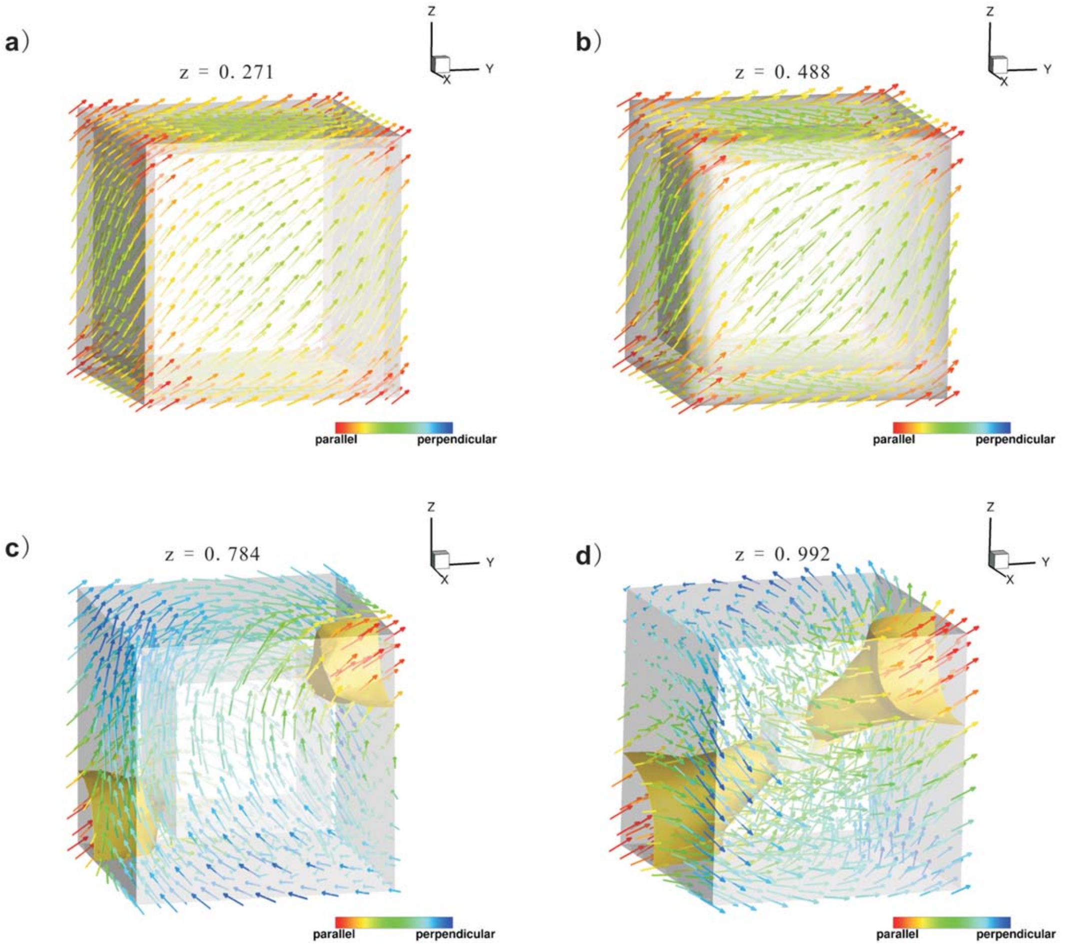

Figure 8. Zero-field micromagnetic domain structures for shell-only model with grain size of 80 nm for different oxidation parameter, z, equal to (a) 0.271, (b) 0.488, (c) 0.784, and (d) 0.992, with initial saturated field along the [111] direction. All structures share the same color coding, with magnetization of elements aligned parallel with the net remanence being red and perpendicular being blue. Translucent isosurfaces (in yellow) have been drawn in Figures 8c and 8d for illustrative purposes. They are surfaces containing all moments lying within 20° of the [111] direction.

5. Discussion

5.1. Low-Temperature Oxidation and the Core-Shell Model

Effects of the low-temperature oxidation on fine-grained magnetite particles are related to multiple factors including particle size, distribution, morphology, and the oxidation mode [*Bleil and Petersen*, 1983; *Worm and Banerjee*, 1984; *Zhou et al*., 2001; *Gee and Kent*, 2007]. Therefore, the oxidation state obtained by XRD measurements represents an average for the assembly as a whole, and may explain why no simple relationships of oxidation parameter with respect to heating period could be found in the oxidation process (Table 1). In this study, various degrees of oxidation for magnetic powders were obtained by comprehensively varying the heating temperature and durations with controlled gas mixture, and were also verified by the gradual shift of the diffraction peaks from magnetite to maghemite (Figure 3).

Our experimental results demonstrate that the hysteresis parameters B_c and M_{rs}/M_s, versus oxidation parameter z exhibit similar trends (Figures 4 and 5). Similar behavior is also reported in a study by *Özdemir and O'Reilly* [1982] for oxidation of titanomagnetites. In that study, they found that the stability of remanence is initially increased by maghemitization (up to $z = \sim 0.4$), and thereafter falls rapidly. They also dismissed a possible explanation of oxidation causing grain division into less stable superparamagnetic sized particles as implausible, because this would result in a decrease in the ratio of M_{rs}/M_s which was not observed. Instead, they suggested that the change in magnetic properties was due to both chemical composition and mineral microstructure.

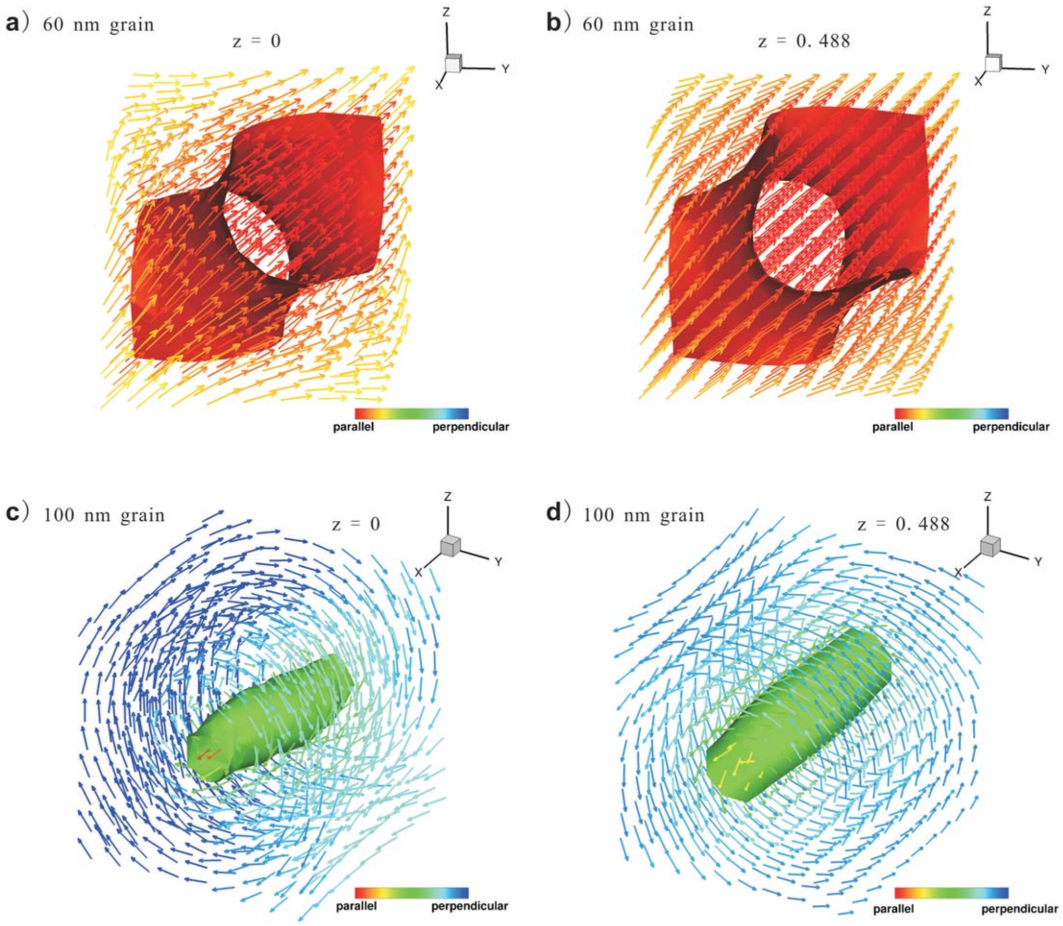

Figure 9. Zero-field micromagnetic domain structures for core-shell model with grain size of (a and b) 60 nm and (c and d) 100 nm for reduced magnetite and surface oxidized magnetite at z = 0.49 with initial field along the [111] direction. All structures share the same color coding as Figure 8. Translucent isosurfaces have been drawn for illustrative purposes, colored red (Figures 9a and 9b) and green (Figures 9c and 9d). They are surfaces containing all moments lying within 5° of the [111] direction (Figures 9a and 9b) and 40° of the [100] direction (Figures 9c and 9d), respectively.

In this study, the magnetic domain structure of the multiphase material was simulated using a simple core-shell micromagnetic model. Even though this model neglects effects of stress that will inevitably be present at the core-shell interface due to the mismatch of the crystal unit cell for the different phases, and also assumes a sharp phase boundary with a material average exchange coupling, the predictions of the model provide a good fit to the experimentally observed trends in the hysteresis properties during maghemitization.

It is clearly shown that reducing the exchange coupling to zero at the phase interface, so that the core and shell only coupled through magnetostatic interactions (Figures 7a and 7b), produces negative coercivities and hysteresis behavior that is not observed experimentally, and thus as expected, some degree of exchange coupling between the core and shell must exist. The micromagnetic model also suggests that the sharp decrease of the hysteresis parameters just before oxidizing to maghemite is most likely due to the change in domain structure in PSD grains as the magnetite inner core is eliminated (Figures 5 and 10), and this is discussed further in the next section.

5.2. The Core-shell Coupling as a Function of Grain Size

It can be seen from Table 2 that magnetocrystalline anisotropy for magnetite is almost three times stronger than its value in maghemite, and so we expect maghemite to be magnetically softer and likely to form less uniform magnetic structures. The hysteresis properties exhibited by the micromagnetic models and

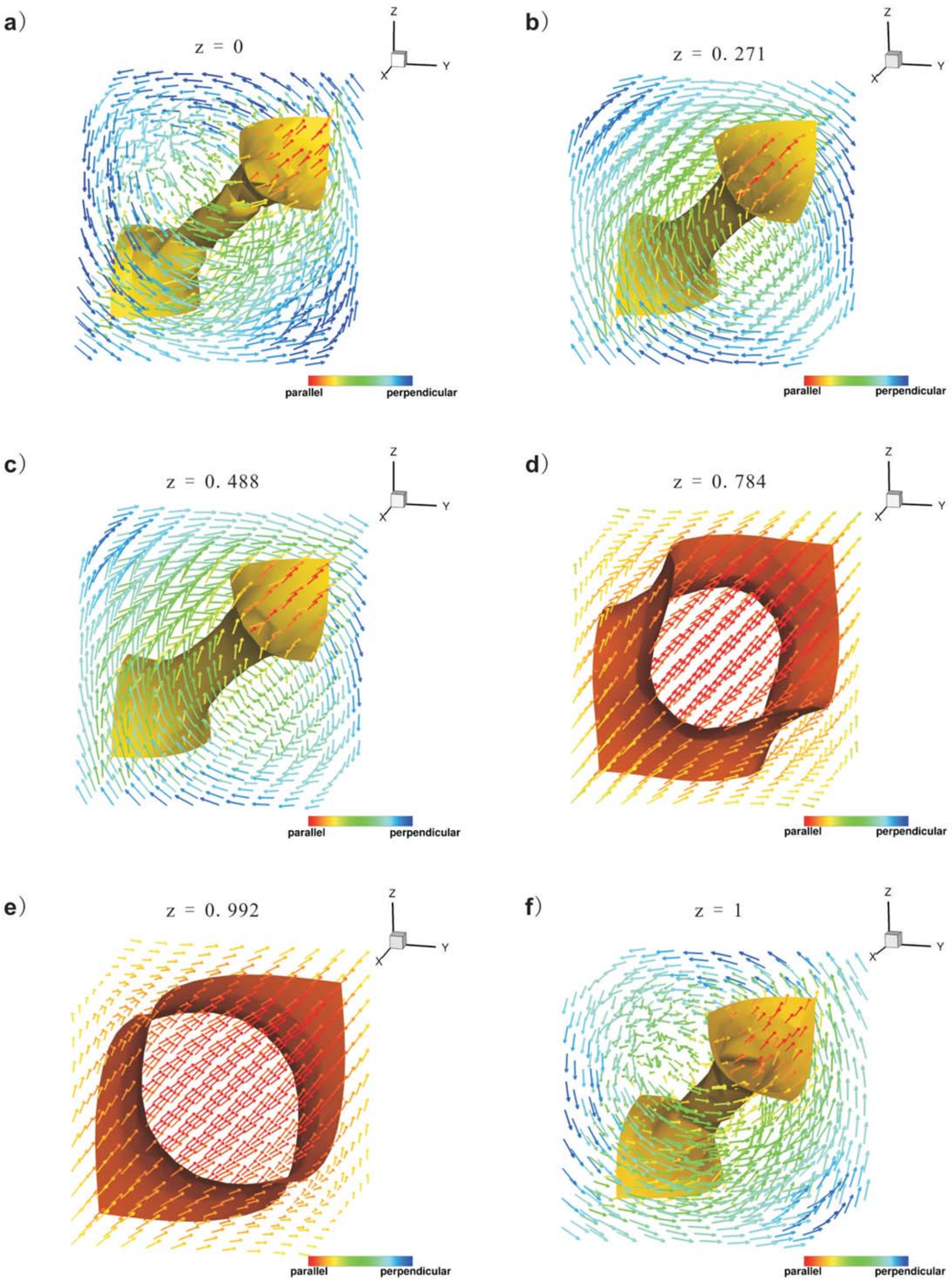

Figure 10. Zero-field micromagnetic domain structures for grain size of 80 nm with oxidation parameter, z, equal to (a) 0, (b) 0.271, (c) 0.488, (d) 0.784, (e) 0.992, and (f) 1. For each model, the sample's magnetizations was saturated along the [111] direction. All structures share the same color coding of magnetization as Figure 8. Translucent isosurfaces have been drawn for illustrative purposes. They are surfaces containing all moments lying within 20° of the [111] direction in Figures 10a–10c, and 10f and 10° in Figures 10d and 10e, respectively.

observed in the experimental observations can be explained in terms of a magnetically softer (lower coercivity) outer shell exchange coupled to a magnetically harder (higher coercivity) inner core.

1. For SD particles (< 70 nm), we observed a high remanence value, but a steady decrease in coercivity as maghemitization increases. The interpretation in this case is straightforward. The domain structures of

both the core and skin implicated in Figure 6 remain in a largely uniform domain state for all values of z. The harder magnetite core undoubtedly imparts a greater coercivity to the whole grain since the switching of the maghemite skin is largely controlled through exchange coupling to the magnetite core. As oxidation proceeds, the softer maghemite gradually dominates producing a lower overall coercivity for the particle.

2. For PSD grains near the critical SD grain size boundary (80 to 100 nm), a more complex hysteresis behavior is observed. The reasons for this can be seen from examining the domain states shown in Figure 10. For example, a 80 nm cubic grain of magnetite will have a vortex minimum energy domain state. However, as oxidation proceeds, the magnetite core shrinks, and the overall magnetic strength of the grain is reduced due to the lower M_s of the maghemite skin. At the same time, a high magnetocrystalline anisotropy remains due to the exchange coupling of the magnetite core to the maghemite skin. Under these conditions of high anisotropy and lower magnetization strength, the minimum energy domain structure is now SD. As oxidation proceeds further, at some point close to complete maghemitization, the small magnetite core shrinks sufficiently so that it is unable to provide a significant influence of the gains' coercivity, and a dramatic collapse in both H_c and M_{rs} is observed as the grain reverts to a vortex domains structure (Figures 7 and 10). Although the overall trend is somewhat obscured by domain state transitions as a function of oxidation, the general picture remains of a gradual magnetic hardening due to a reduction of magnetization as the maghemite skin grows. This trend continues until the core disappears upon complete maghematization.

3. Finally, for larger PSD grains, well away from the critical SD grain size boundary ($>$ 110 nm) the grains will remain in a vortex state throughout the oxidation process. Nevertheless, the physical mechanism of magnetic hardening with oxidation still prevails. The effect in this case, however, is to simply reduce the vorticity of the magnetic domain state as the maghemite skin grows (Figures 9c and 9d). The magnetically harder and slightly more uniform domain structures result in a trend of increasing M_{rs} and B_c until the magnetite core almost disappears when both parameters decrease significantly.

5.3. Implications for Palaeomagnetic Studies

In palaeomagnetism and environmental magnetism, magnetite grains in the transitional range between SD and small PSD particles are of paramount importance, because of their high remanence intensity and stability, and their ability to reliably record the geomagnetic field. Our experiments indicate that both B_c and M_{rs}/M_s increase significantly as the surface oxidation grows to $\sim$0.9, which means these partially oxidized particles are also capable of holding a stable remanence [*Williams et al*., 2011]. As anticipated, the domain structures derived from the micromagnetic models show that the remanence and its net direction for the oxidized particles in the SD and PSD grain size range will have little modification with oxidation except for a narrow range of particles sizes near the critic SD grain size boundary (Figures 7–9). In other words, most particles can still hold a stable paleodirection and paleointensity despite having suffered from chemical alteration. Although the magnetization direction of most SD and PSD grains will not change, the remanence may enhance slightly with mineral transformation. Nevertheless, our study suggests that surface oxidized magnetite in SD-PSD range can reliably record a palaeomagnetic signal.

The low-temperature oxidation of magnetite to maghemite and the corresponding oxidation of titanomagnetite to titanomaghemite are ubiquitous in surface-weathered continental rocks and altered seafloor basalts. In this two-phase transformation process, there is no doubt that the new secondary mineral will be influenced by the primary phase, making a simple block theory of chemical remanence magnetization (CRM) no longer hold [*Moskowitz*, 1980]. However, although the long-time oxidation of magnetic minerals that occur during periods of geomagnetic reversals or transitions should also be investigated carefully, low-temperature oxidation of magnetite or titanomagnetite that are exposed in a stable magnetic field, e.g., Cretaceous normal superchron (CNS), should record reliable magnetic signals. For example, *Bleil and Petersen* [1983] reported a steady increase of remanence of ocean floor basalts from the age of 20 Ma up to $\sim$120 Ma, corresponding to increasing degrees of oxidation. These basalts could be explained well by the slight increase of hysteresis parameters with the increase of oxidation parameter (Figures 5 and 10), and should still be good geomagnetic recorders. This study also indicates that the paleointensity can be recorded reasonably well by using magnetofossils in sediment, which may consist of concentrated SD magnetic grains. It is clear that CRM acquired during low-temperature oxidation is likely to be a reliable source of magnetic recorders.

5.4. Further Studies

The predicted results are in good agreement with the experimental observations (Figure 7). However, some differences are also observed. For example, the experimental results (Figure 5) for reduced powders have higher coercive values (∼18 mT) and lower values of M_{rs}/M_s (∼0.22) compared to the predictions of numerical models (∼10 mT and ∼0.27, respectively, for weighted values of models with exchange value of 1.17×10^{-11} J m^{-1} at the interface).

Although our model accounts for average idealized mineral compositions produced during surface or seafloor weathering, the changes in microstucture (e.g., due to grain cracking or heterogeneities) which may occur in nature are not reproduced. Some differences may be attributed to averaging of PSD and SD characteristics and some variation in oxidation levels with the grain-size distribution of the experimental sample (Figures 5a, 7c, and 7e). A simple weighted average of all modeling results based on the distribution of experiment samples may not be sufficient because of the existence of interactions and neglect of random crystalline anisotropy. There may be an underestimation of the oxidation parameter determined by XRD method in the earlier oxidation, because of the shallow shell and our assumption of a sharp rather than continuous transition zone (D. J. Dunlop, personal communication, 2012). It is also possible that the existence of superparamagnetic and large PSD grains in the experimental samples might contribute to a decrease in the observed values of M_{rs}/M_s [*Tauxe et al*., 2002]. In addition, impurities and uncertainties of interparticle magnetostatic interactions (despite our best efforts of particle dispersion), which may exist in both synthetic and natural samples, might also influence the consistency between the experiments and the simulation.

More significantly, we may expect difference in absolute values of hysteresis parameters due to the simple nature of the micromagnetic model. The model considers only grains of symmetrical cubic geometry and that have a uniformly oxidized skin (Figure 2). It neglects the effects of stress and thermal fluctuations and assumes a sharp boundary between the core and oxidized skin. Nevertheless, the model is sufficient to demonstrate the mechanism of magnetic hardening in PSD grains caused by the high magnetocrystalline anisotropy magnetite core exchange coupled to the softer maghemite skin.

Further studies should be conducted on natural samples and may bridge this gap as well as exploring the effects of shape anisotropy [*Tauxe et al*., 2002; *Yu and Tauxe*, 2008], and that of a transition zone at the oxidation interface [*Özdemir and Dunlop*, 2010].

6. Conclusions

Surface oxidized magnetite powders of different states were systematically produced by heating at different temperatures and for various durations. The experimental properties were subsequently obtained through careful bulk magnetic measurements. Micromagnetic simulations were performed to investigate the hysteresis parameters versus the oxidation state using a simple exchange coupled core-shell model. These results show a range of different magnetic behaviors for partially oxidized grains and for various grain sizes, which are in good agreement with the observation on our experimental sample containing SD and PSD grains. We conclude that the magnetic properties of surface oxidized magnetite are likely to be dominated by an exchange coupled core-shell structure and that low-temperature oxidized magnetite in SD-PSD range can reliably record palaeomagnetic signals.

Acknowledgments
This work was supported by the National Natural Science Foundation of China (NSFC grants 41374073 and 41025013) and Chinese Academy of Sciences. We also acknowledge the support of NERC research grant NE/H006508/1 to W.W. The authors are very grateful to Shanke Liu for the XRD analysis. We are also wishing to thank David Dunlop and Özden Özdemir for helpful suggestions and comments on the discussion. We further thank R. van der Voo, an anonymous reviewer and the Associated Editor J. Feinberg for their helpful comments.

References

Askill, J. (1970), *Tracer Diffusion Data for Metals, Alloys, and Simple Oxides*, 97 pp., Plenum, New York.

Banerjee, S., J. King, and J. Marvin (1981), A rapid method for magnetic granulometry with applications to environmental studies, *Geophys. Res. Lett.*, *8*(4), 333–336.

Bleil, U., and N. Petersen (1983), Variations in magnetization intensity and low-temperature titanomagnetite oxidation of ocean floor basalts. *Nature*, *301*, 384–388.

Brown, W. F. (1963), *Micromagnetics*, 147 pp., Interscience, New York.

Cui, Y., K. L. Verosub, and A. P. Roberts (1994), The effect of low-temperature oxidation on large multi-domain magnetite, *Geophys. Res. Lett.*, *21*(9), 757–760.

Dunlop, D. J., and Ö. Özdemir (2001), *Rock Magnetism: Fundamentals and Frontiers*, 577 pp., Cambridge Univ. Press, New York.

Fabian, K., A. Kirchner, W. Williams, F. Heider, T. Leibl, and A. Hubert (1996), Three-dimensional micromagnetic calculations for magnetite using FFT, *Geophys. J. Int.*, *124*(1), 89–104.

Fidler, J., and T. Schrefl (2000), Micromagnetic modelling—The current state of the art, *J. Phys. D Appl. Phys.*, *33*, R135, doi:10.1088/0022–3727/33/15/201.

Fukuma, K., and D. J. Dunlop (2006), Three-dimensional micromagnetic modeling of randomly oriented magnetite grains (0.03-0.3 mm), *J. Geophys. Res.*, *111*, B12S11, doi:10.1029/2006JB004562.

Gallagher, K. (1968), Mechanism of oxidation of magnetite to gamma-Fe_2O_3, *Nature*, *217*, 1118–1121.

Gee, J. S., and D. V. Kent (2007), Source of oceanic magnetic anomalies and the geomagnetic polarity time scale, *Treatise Geophys.*, *5*, 455-507.

Haneda, K., and A. Morrish (1977), Magnetite to maghemite transformation in ultrafine particles, *J. Phys. Colloq.*, *38*(C1), C1-321-C321-323, doi:10.1051/jphyscol:1977166.

Heider, F., and W. Williams (1988), Note on temperature-dependence of exchange constant in magnetite, *Geophys. Res. Lett.*, *15*(2), 184–187.

Hou, D., X. Nie, and H. Luo (1998), Studies on the magnetic viscosity and the magnetic anisotropy of γ-Fe_2O_3 powders, *Appl. Phys. A*, *66*(1), 109–114.

Johnson, H., and R. Merrill (1972), Magnetic and mineralogical changes associated with low-temperature oxidation of magnetite, *J. Geophys. Res.*, *77*(2), 334–341.

Johnson, H. P., and R. T. Merrill (1973), Low-temperature oxidation of a titano- magnetite and implications for palaeomagnetism, *J. Geophys. Res.*, *78*(23), 4938–4949.

Johnson, H., and R. Merrill (1974), Low-temperature oxidation of a single-domain magnetite, *J. Geophys. Res.*, *79*(35), 5533–5534.

Liu, C. C., C. L. Deng, Q. S. Liu, L. T. Zheng, W. Wang, X. M. Xu, S. Huang, and B. Y. Yuan (2010), Mineral magnetism to probe into the nature of palaeomagnetic signals of subtropical red soil sequences in southern China, *Geophys. J. Int.*, *181*(3), 1395–1410.

Liu, C. Y., K. P. Ge, C. X. Zhang, Q. S. Liu, C. L. Deng, and R. X. Zhu (2011), Nature of remagnetization of Lower Triassic red beds in southwestern China, *Geophys. J. Int.*, *187*(3), 1237–1249.

Liu, Q. S., S. K. Banerjee, M. J. Jackson, C. L. Deng, Y. X. Pan, and R. X. Zhu (2004), New insights into partial oxidation model of magnetites and thermal alteration of magnetic mineralogy of the Chinese loess in air, *Geophys. J. Int.*, *158*(2), 506–514.

Liu, Q. S., C. L. Deng, J. Torrent, and R. X. Zhu (2007), Review of recent developments in mineral magnetism of the Chinese loess, *Quat. Sci. Rev.*, *26*(3–4), 368–385.

Liu, Q. S., P. X. Hu, J. Torrent, V. Barron, X. Y. Zhao, Z. X. Jiang, and Y. L. Su (2010), Environmental magnetic study of a Xeralf chronosequence in northwestern Spain: Indications for pedogenesis, *Palaeogeogr. Palaeoclimatol. Palaeoecol.*, *293*(1–2), 144–156.

Liu Q. S., A. P. Roberts, J. C. Larrasoaña, S. K. Banerjee, Y. Guyodo, L. Tauxe, and F. Oldfield (2012), Environmental magnetism: Principles and applications, *Rev. Geophys.*, *50*, RG4002, doi:10.1029/2012RG000393.

Lu, S. G., D. J. Chen, S. Y. Wang, and Y. D. Liu (2012), Rock magnetism investigation of highly magnetic soil developed on calcareous rock in Yun-Gui Plateau, China: Evidence for pedogenic magnetic minerals, *J. Appl. Geophys.*, *77*, 39–50.

Marshall, M., and A. Cox (1971), Magnetism of pillow basalts and their petrology, *Geol. Soc. Am. Bull.*, *82*(3), 537–552.

Moskowitz, B. M. (1980), Theoretical grain size limits for single-domain, pseudo-single-domain and multi-domain behavior in titanomagnetite ($x = 0.6$) as a function of low-temperature oxidation, *Earth Planet. Sci. Lett.*, *47*(2), 285–293.

Muxworthy, A., W. Williams, and D. Virdee (2003), Effect of magnetostatic interactions on the hysteresis parameters of single-domain and pseudo-single-domain grains, *J. Geophys. Res.*, *108*(B11), 2517, doi:10.1029/2003JB002588.

Muxworthy, A., D. Heslop, and W. Williams (2004), Influence of magnetostatic interactions on first-order-reversal-curve (FORC) diagrams: a micromagnetic approach, *Geophys. J. Int.*, *158*(3), 888–897.

Muxworthy, A. R., and W. Williams (2006), Critical single-domain/multidomain grain sizes in noninteracting and interacting elongated magnetite particles: implications for magnetosomes, *J. Geophys. Res.*, *111*, B12S12, doi:10.1029/2006JB004588.

O'Reilly, W. (1984), *Rock and Mineral Magnetism*, 220 pp., Blackie Acad. and Prof, Glasgow, U. K.

Özdemir, Ö., and D. J. Dunlop (1985), An experimental-study of chemical remanent magnetizations of synthetic monodomain titanomaghemits with initial thermoremanent magnetizations, *J. Geophys. Res.*, *90*(13), 1513–1523.

Özdemir, Ö., and D. J. Dunlop (2010), Hallmarks of maghemitization in low-temperature remanence cycling of partially oxidized magnetite nanoparticles, *J. Geophys. Res.*, *115*, B02101, doi:10.1029/2009JB006756.

Özdemir, Ö., D. J. Dunlop, and B. M. Moskowitz (1993), The effect of oxidation on the Verwey transition in magnetite, *Geophys. Res. Lett.*, *20*(16), 1671–1674.

Özdemir, Ö., and W. O'Reilly (1982), Magnetic hysteresis properties of synthetic monodomain titanomaghemites, *Earth Planet. Sci. Lett.*, *57*(2), 437–447.

Pauthenet, R., and L. Bochirol (1951), Aimantation spontanée des ferrites, *J. Phys. Radium*, *12*(3), 249–251.

Prévot, M., A. Lecaille, and E. A. Mankinen (1981), Magnetic effects of maghem- itization of oceanic crust, *J. Geophys. Res.*, *86*(B5), 4009–4020.

Readman, P., and W. O'Reilly (1971), Oxidation processes in titanomagnetites, *Z. Geophys.*, *37*(3), 329–338.

Readman, P., and W. O'Reilly (1972), Magnetic properties of oxidized (cation-deficient) titanomagnetites $(Fe, Ti, \square)_3O4$, *J. Geomagn. Geoelectr.*, *24*(1), 69–90.

Rietveld, H. (1969), A profile refinement method for nuclear and magnetic structures, *J. Appl. Crystallogr.*, *2*(2), 65–71.

Schabes, M. E., H. N. Bertram (1988), Magnetization processes in ferromagnetic cubes. *J. Appl. Phys.*, *64*(3), 1347–1357.

Smith, B. M. (1987), Consequences of the maghemitization on the magnetic-properties of submarine basalts—synthesis of previous works and results concerning basement rocks from mainly Dsdp Leg-51 and Leg-52, *Phys. Earth Planet. Inter.*, *46*(1–3), 206–226.

Tauxe, L., H. N. Bertram, and C. Seberino (2002), Physical interpretation of hysteresis loops: Micromagnetic modeling of fine particle magnetite, *Geochem. Geophys. Geosyst.*, *3*(10), 1055, doi:10.1029/2001GC000241.

van Velzen, A. J., and M. J. Dekkers (1999), Low-temperature oxidation of magnetite in loess-palaeosol sequences: A correction of rock magnetic parameters, *Stud. Geophys. Geod.*, *43*(4), 357–375.

Wang, D., R. Van der Voo, and D. R. Peacor (2006), Low-temperature alteration and magnetic changes of variably altered pillow basalts, *Geophys. J. Int.*, *164*(1), 25–35.

Watkins, N. (1967), Unstable components and palaeomagnetic evidence for a geomagnetic polarity transition, *J. Geomagn. Geoelectr.*, *19*, 63–76.

Williams, W., and D. J. Dunlop (1989), Three-dimensional micromagnetic modelling of ferromagnetic domain structure, *Nature*, *337*(6208), 634–637.

Williams, W., and D. J. Dunlop (1995), Simulation of magnetic hysteresis in pseudo- single-domain grains of magnetite, *J. Geophys. Res.*, *100*, 3859–3871.

Williams, W., A. R. Muxworthy, and G. A. Paterson (2006), Configurational anisotropy in single-domain and pseudosingle-domain grains of magnetite, *J. Geophys. Res.*, *111*, B12S13, doi:10.1029/2006JB004556.

Williams, W., M. E. Evans, and D. Krása (2010), Micromagnetics of palaeomagnetically significant mineral grains with complex morphology, *Geochem. Geophys. Geosyst.*, *11*, Q02Z14, doi:10.1029/2009GC002828.

Williams, W., A. Muxworthy, and M. Evans (2011), A micromagnetic investigation of magnetite grains in the form of Platonic polyhedra with surface roughness, *Geochem. Geophys. Geosyst.*, *12*, Q10Z31, doi:10.1029/2011GC003560.

Witt, A., K. Fabian, and U. Bleil (2005), Three-dimensional micromagnetic calculations for naturally shaped magnetite: Octahedra and magnetosomes, *Earth Planet. Sci. Lett.*, *233*, 311–324.

Worm, H. U., and S. K. Banerjee (1984), Aqueous low-temperature oxidation of titanomagnetite, *Geophys. Res. Lett.*, *11*(3), 169–172.

Xu, W., R. Van der Voo, D. R. Peacor, and R. T. Beaubouef (1997), Alteration and dissolution of fine-grained magnetite and its effects on magnetization of the ocean floor, *Earth Planet. Sci. Lett.*, *151*(3), 279–288.

Yu, Y., and L. Tauxe (2005), On the use of magnetic transient hysteresis in palaeomagnetism for granulometry. *Geochem. Geophys. Geosyst.*, *6*(1), Q01H14, doi:10.1029/2004GC000839.

Yu, Y., and L. Tauxe (2008), Micromagnetic models of the effect of particle shape on magnetic hysteresis, *Phys. Earth Planet. Inter.*, *169*, 92–99.

Zhou, W., R. Van der Voo, D. R. Peacor, D. Wang, and Y. Zhang (2001), Low-temperature oxidation in MORB of titanomagnetite to titanomaghemite: A gradual process with implications for marine magnetic anomaly amplitudes, *J. Geophys. Res.*, *106*(B4), 6409–6421.